

SWAG: Long-term Surgical Workflow Prediction with Generative-based Anticipation

Maxence Boels*, Yang Liu, Prokar Dasgupta,
Alejandro Granados, Sebastien Ourselin

Surgical and Interventional Engineering, King’s College London.

*Corresponding author(s). E-mail(s): maxence.boels@kcl.ac.uk;

Abstract

Purpose While existing approaches excel at recognising current surgical phases, they provide limited foresight and intraoperative guidance into future procedural steps. Similarly, current anticipation methods are constrained to predicting short-term and singular events, neglecting the dense and sequential nature of surgical workflows. To address these needs and limitations, we propose SWAG (Surgical Workflow Anticipative Generation), a framework to combine phase recognition and anticipation, using a generative approach for surgical workflow guidance.

Methods This paper investigates two distinct decoding methods—single-pass (SP) and auto-regressive (AR)—to generate sequences of future surgical phases at minute intervals over long horizons of up to 60 minutes. We propose a novel embedding approach using prior knowledge to enhance the accuracy of phase anticipation. Additionally, our anticipative framework offers remaining time regression and proposes a regression-to-classification (R2C) method. SWAG’s performance was evaluated on the Cholec80 and AutoLaparo21 datasets.

Results Our single-pass model with prior knowledge embeddings (SP*) achieves 49.8% mean accuracy over 18-minute anticipation on AutoLaparo21, while the simple SP with R2C extension reaches 56.6% mean accuracy over the same horizon on Cholec80. Moreover, our approach outperforms existing methods on the phase remaining time regression task, achieving weighted mean absolute errors of 0.32 and 0.48 minutes for 2- and 3-minute horizons, respectively.

Conclusion SWAG demonstrates versatility across classification and regression tasks and creates a temporal continuity between surgical workflow recognition and anticipation. While further studies are required to understand the impact of generative-based anticipation intraoperatively, our method provides steps towards this direction. Project: <https://maxboels.github.io/swag>.

Keywords: Surgical Workflow Anticipation, Surgical Phase Recognition, Surgical Workflow Generation, Remaining Time Regression, Cholec80, AutoLaparo21

1 Introduction

SURGICAL WORKFLOW ANTICIPATION has the potential to enhance operating room efficiency and patient safety by predicting future surgical events during procedures. Anticipation allows for better preparation, reduces cognitive loads, and improves coordination among surgical teams [1, 2]. While preoperative planning provides an initial framework, it often falls short in addressing the dynamic environment and decision-making required during surgery.

Current approaches predominantly focus on surgical phase recognition, identifying the present phase, step, or action [3–5]. These methods are valuable for postoperative analysis but offer limited assistance in real-time intraoperative decision-making. They cannot anticipate future events to allow for dynamic planning adjustments, which could potentially improve surgical outcomes. Remaining Surgery Duration (RSD) estimation has been actively researched for over two decades [6–11], demonstrating clinical interest in long-term predictions—i.e. predicting the remaining time until the end of the surgery. Other studies explore surgical workflow anticipation, such as predicting the next phases and instrument occurrences [12, 13]. However, these methods are limited by their requirement to predict a single event per class, disregarding scenarios where multiple future occurrences may exist within a fixed time horizon.

Generative models, such as GPT models [14], address this challenge by generating sequences of tokens that can vary in both length and class frequency. In surgical workflow anticipation, auto-regressive (AR) [14] and single-pass (SP) decoding models [15] demonstrate the potential to predict continuous, coherent sequences of surgical actions. Unlike conventional remaining time regression approaches, generative models output multiple tokens, extending the observed sequence of events to a plausible future representation of the surgical workflow.

In this work, we present SWAG (Surgical Workflow Anticipative Generation), a generative model designed to unify phase recognition and anticipation in surgical workflows. Our main contributions are as follows:

1. We introduce SWAG, a generative model that combines surgical phase recognition and anticipation for long-term and dense future prediction of workflows.
2. We provide an extensive comparison of two generative decoding methods—single-pass and auto-regressive—alongside two tasks—classification and regression—to generate sequences of future surgical phases.
3. We propose a novel prior knowledge embedding mechanism using class-conditional probabilities to initialise the input tokens, enhancing anticipation accuracy.
4. We conduct a comprehensive evaluation on the Cholec80 and AutoLaparo21 datasets, demonstrating SWAG’s performances on different surgical procedures.

2 Related Work

Surgical Phase Recognition. Early research on surgical phase recognition relied on probabilistic graphical models with instrument usage [16]. Later, convolutional neural networks were used to learn spatial representations from surgical video frames,

while temporal relations among video frames were captured with recurrent neural networks [17]. Temporal convolutional networks were later able to increase the receptive field [3]. Recent works have successfully used Transformers [18, 19] to capture critical information between frames using short attention windows like in Trans-SVNet [20] and LoViT [4], whereas SKiT [5] proposed an efficient long-term compression approach achieving state-of-the-art performance on online surgical phase recognition. SAHC [21] proposes to model surgical workflows at both frame and segment levels to better capture phase transitions. Limitations between anticipation and batch normalisation for surgical workflow analysis are presented in BNPFalls [22]. SurgFormer [23] introduces a transformer architecture with hierarchical temporal attention for phase recognition. Although these approaches offer substantial advancements for postoperative video analysis, we focus on intraoperative decision-making by adding anticipative capabilities to the recognition system. Anticipating the surgical workflow over long time horizons could enhance real-time decision support by forecasting upcoming surgical phases, enabling smoother, more responsive guidance during procedures.

Surgical Workflow Anticipation. Most anticipation approaches in surgery have explored surgical workflow anticipation by predicting the remaining time until the end of surgery [6–11], next instruments [12] or next phases occurrence [13, 24, 25]. Bayesian [12] was proposed to anticipate tool usage which was then used as a baseline in IIA-Net [13] for surgical phase anticipation. IIA-Net [13] was then introduced to leverage instrument interaction for next-phase occurrence regression. Although IIA-Net requires pre-trained models for tool detection and segmentation, we compare our method to this approach and their implementation of Bayesian [12]. Both methods were formulated as a regression problem, for surgical phase anticipation. SUPR-GAN [24] uses LSTMs within an encoder-decoder architecture to predict surgical phases over 15 seconds. A discriminator is used to train the model, using a generative adversarial network (GAN) approach. In contrast, our SWAG model addresses long-term surgical workflow anticipation, predicting sequences up to 60 minutes while unifying recognition and anticipation tasks. Zhang et al. [26] proposes a graph network with bounding boxes as inputs to predict the occurrence of instruments or phases within 2-, 3-, and 5-minute horizons. Later, Hypergraph-Transformer (HGT) was proposed in [27] to detect and predict action triplets over 4 seconds. Other methods were also proposed for gesture anticipation as low-level motion planning [28], instrument trajectory prediction [29, 30]. Most methods focus on the next occurrence regression, failing to provide a comprehensive view of the entire surgical workflow, leaving a blind spot for events beyond the first predicted occurrence. Unlike previous works, SWAG uses a generative approach for future phase classification. Our approach addresses some gaps and limitations by predicting sequences of arbitrary length and frequency, and unifying recognition and anticipation tasks.

3 Methods

In this section, we present our proposed method for jointly addressing surgical phase recognition and anticipation. Our model, SWAG, is designed to predict the current phase while anticipating the occurrence of future phases over long-time horizons.

3.1 Task Formulation

Our primary task is to predict future surgical phases over a horizon of $H = 60$ minutes, conditioned on observed frames $X_t = \{x_0, \dots, x_t\}$ where $x_i \in \mathcal{X}_T$ (all video frames). We define the mapping function as follows:

$$f_\theta : x_{\leq t} \mapsto (y_{t+n_1 \cdot 60}, \dots, y_{t+n_H \cdot 60}) \quad (1)$$

where $x_{\leq t}$ denotes the sequence of frames up to time t . The anticipation indices n_i range from 1 to H , corresponding to the number of minutes into the future for which we predict the surgical phase $y_{t+n_i \cdot 60}$.

For regression, we predict the remaining time until each phase’s next occurrence within $[0, H]$ minutes, where 0 indicates the phase is currently active, and H means it will not occur within the horizon. Our setup follows [12, 13]. We predict phases every 60 seconds based on our ablations (see Fig. 2 in SM).

3.2 SWAG Model Architecture

Our proposed model, illustrated in Figure 1, comprises a Vision Encoder followed by a Windowed Self-Attention encoder (WSA), then a linear Compression and max-Pooling mechanisms (CP) [5], and finally a future Decoder module that can operate either in a single-pass (SP) or an auto-regressive (AR) approach. While our model uses classification for the phase recognition task, it can use classification or regression for phase anticipation. This architecture also includes a novel Prior Knowledge Embedding relying on the predicted class \hat{y}_0 at anticipation index 0 and the index position of the anticipated time horizons \mathcal{N}_H .

Vision Encoder. Similar to LoViT, we fine-tune a pre-trained ViT [19] using the AVT [31] approach, which trains on short segments of consecutive frames. This procedure allows the model to incorporate limited temporal context while learning spatial features. At inference, we then extract a single 768-dimensional embedding per frame f_t , serving as the initial feature representation.

Window Self-Attention (WSA). To recognise the observed frame at time t , we use an input $F_t = \{f_{t-l}, \dots, f_t\}$ of length $l = 1440$ s or 24 minutes and latent representations with $d = 768$ dimensions. We then use a short sliding window of width $w = 20$ s to perform self-attention over the input sequence with no overlap and get an output sequence of the same length and dimensionality, $E_t = \{e_{t-l}, \dots, e_t\}$.

Compression and Pooling (CP). We evaluate two temporal pooling methods i.e. global key-pooling [5] and our interval-pooling with single-pass and auto-regressive decoders (see Fig. 3 in SM). We select global key-pooling [5] as the best of both methods. This approach compresses the $E_t = \{e_{t-l}, \dots, e_t\}$ features into a lower dimensional latent space $d = 32$ and aggregates long-term information using max-pooling into the last $M = 24$ frame embeddings. A linear layer returns the compressed features to their original dimensionality $D = 512$ as $K_t = \{k_1, \dots, k_M\}$. This bottleneck helps extract global information and passes it to local features [5]. Alternatively, we tried *interval-pooling* that does max-pooling over 60-second intervals to preserve the positional information. This method has a fixed start time at $t-l$, while the right-side index is extended by 60 seconds for each new token, effectively compressing 60

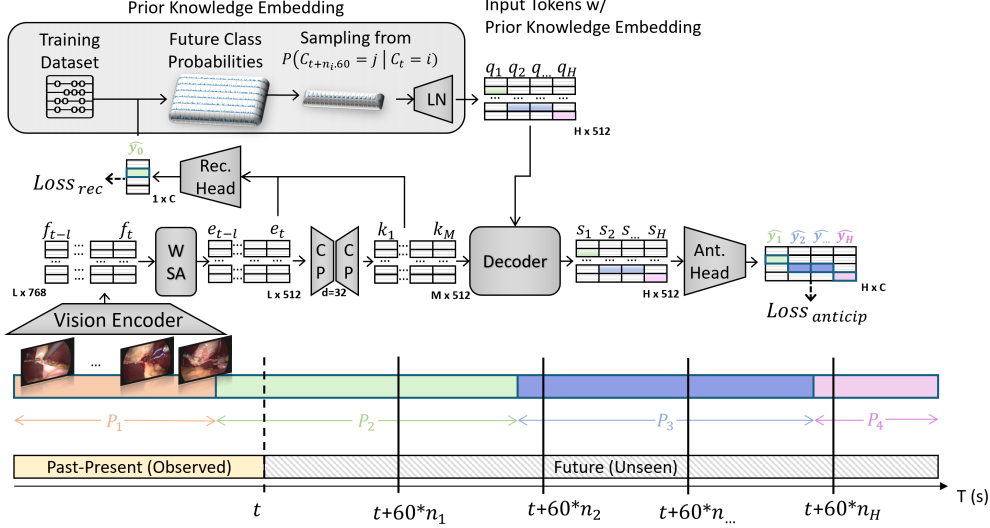


Fig. 1: Overview of the SWAG-SP* model architecture. The model processes surgical video data in two main paths: (1) A recognition path with $L = 24 * 60$ frame embeddings and $M = 24$ compressed frame representations are encoded into $D = 512$ -dimensional embeddings through a Vision Encoder, a Windowed Self-Attention (WSA) encoder and a Compression and max-Pooling (CP) bottleneck to recognise the current surgical phase with a classification head ($Loss_{recognition}$). (2) A generative path samples H times from future class probabilities extracted from the training set. These probabilities are combined with temporal position embeddings to form input tokens $Q_t = \{q_1, q_2, \dots, q_H\}$, and passed to a Decoder that conditions the compressed frame embeddings i.e. context tokens $K_t = \{k_1, k_2, \dots, k_M\}$ to predict H future surgical phases at 60 seconds intervals ($Loss_{anticipation}$). The timeline shows the model operating on past-present observed frames from phases P_1 (orange) and P_2 (green) and predicting probabilities $H \times C$ of future phases.

frame embeddings into a single token, yielding M context tokens. M corresponds to the full length divided by 60-second intervals, therefore compressing 24 minutes into 24 tokens, i.e. $\frac{1440}{60}$.

Decoder. Our two decoding approaches (see Fig. 2) can be described as follows:

1) **SWAG-SP (Single-Pass):** The decoder receives H input tokens $Q_t = \{q_1, \dots, q_H\}$ and generates H output tokens $S_t = \{s_1, \dots, s_H\}$ in a single forward pass, each token represents 60 seconds over H minutes. During training, we use a special teacher-forcing approach, using the ground-truth current phase y_t to sample from the correct prior distributions $P(y_{t+n_i \cdot 60} = j | y_t = i)$ at future minute index n_i , H times. The Q_t inputs are initialized with prior knowledge corresponding to conditional future class probabilities extracted from the training set (see Sec. 1.2 in SM) and sinusoidal positional encoding. This generative approach is conditioned on the M context tokens $K_t = \{k_1, \dots, k_M\}$ once to generate all future tokens S_t , allowing for efficient parallel computing and reducing inference time.

2) **SWAG-AR (Auto-Regressive)**: Our decoder architecture builds upon the GPT-2 framework [14] which takes a single input sequence K_t , and predicts the next token with masked self-attention. Teacher forcing is not used as our approach uses the M learned frame embeddings from the recognition channel rather than embedding ground-truth labels into inputs. SWAG-AR uses M context tokens as input, with predictions for k_{t+1} conditioned on the spatiotemporal context tokens $K_t = \{k_1, \dots, k_M\}$. This context token decoding method iteratively expands during inference until generating all H future tokens.

Recognition Head (Rec. Head). We first fuse the key-pooled features K_t with the windowed self-attention features $E_t = \{e_{t-M}, \dots, e_t\}$ using a skip connection [5]. The resulting fused feature vectors are then passed through a classification layer to predict the future M class probabilities for $\{\hat{p}_1, \dots, \hat{p}_M\}$. The final prediction \hat{y}_0 for frame x_t , takes the last frame’s class probabilities, \hat{p}_t .

Anticipation Head (Ant. Head). The future phase classification task predicts outputs with shape $H \times C$, with $\{\hat{p}_1, \dots, \hat{p}_H\}$. The final linear layer (LN) \hat{y}_0 for frame x_t , takes the last frame’s class probabilities, \hat{p}_t .

Note that, the regression task outputs $1 \times C$ values for the remaining time until the next phases, including the end-of-surgery (eos) class. While remaining time regression could be performed via auto-regressive decoding with a single iteration, we opt for a single-pass decoder since a single token can represent specific transitions over time, and also due to the stronger performance on the classification task. Nevertheless, future work could explore generating multiple transitions per class (e.g., one for each auto-regressively generated token) to narrow potential performance gaps relative to an SP scheme.

SWAG-SP* (with Prior Knowledge Embedding). Our extracted prior knowledge captures the conditional probabilities of phase transitions, derived exclusively from the training set. Specifically, we compute the probability of transitioning from the current class i at time t to future classes j at different anticipation times $t + n_i \cdot 60$, denoted as $P(y_{t+n_i \cdot 60} = j \mid y_t = i)$. These probabilities form a tensor P , where each entry $P_{i,j,n_i \cdot 60}$ represents the likelihood of transitioning between classes at each anticipation time. We use these distributions to initialise future token embeddings, assigning each future token at $t + n_i \cdot 60$ the probability vector $P_{i,:,n_i \cdot 60}$. While these priors are specific to each surgical procedure type, they could potentially be transferred between similar procedures, which we plan to investigate in future work.

SWAG-SP-R2C (Regression-to-Classification). We demonstrate a possible mapping from regression outputs to classification via our *regression-to-classification (R2C)* method, which converts continuous time predictions into discrete phase intervals by sorting and binning predicted times. This approach can be used if one wishes to derive a phase sequence from a model originally trained for regression. Specifically, remaining time predictions are mapped to a discrete sequence of H bins containing the future H predicted class integers $Y_t = \{\hat{y}_1, \dots, \hat{y}_H\}$, in ascending order of occurrence. We use the current predicted class \hat{y}_0 to fill the sequence up to \hat{y}_1 .

We use cross-entropy and mean squared error losses for the classification and regression tasks, respectively.

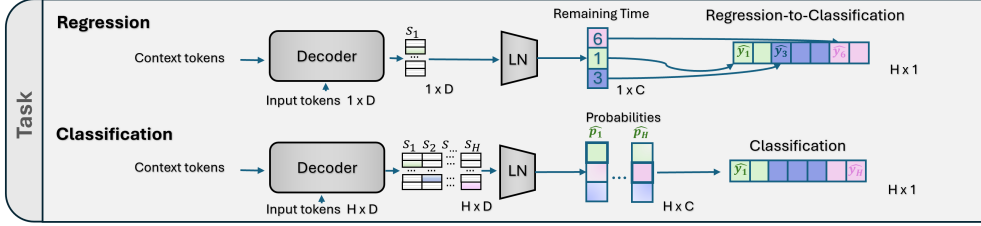


Fig. 2: Single-Pass regression and classification tasks. The regression task (top) uses a single $1 \times D$ input token to predict the remaining time before each next class occurrence, which can be transformed into a classification task using our Regression-to-Classification (R2C) method. The direct classification task (bottom) uses H input tokens to predict H minutes in the future.

3.3 Experimental Setup

Datasets. We evaluate our work on two publicly available surgical phase datasets: *Cholec80* (C80) [32] and *AutoLaparo21* (AL21) [33]. For C80, we follow the 40/40 train-test split for classification as in [4, 20], and for the regression task, we use the 60/20 train-test split following [12, 13]. For AL21, we follow the same 14/7 split for training and testing as in [4]. Both datasets were sampled at 1 frame per second (fps) following previous works [4, 20]. Across both datasets, we train on the 7 surgical phases, including an additional end-of-surgery (EOS) class, while disregarding tool annotations.

Training Details. We train a single model on a maximal horizon $H = 60$ minutes and evaluate it at intermediate steps without re-training. We use a simple cross-entropy loss for the anticipation task and mean squared error loss for the regression task. Additional details on the training procedure are provided in the supplementary material (Sec. 1.1 in SM).

Anticipation Time. We assess our method over a range of intermediate horizons to capture both short-term (2, 3, and 5 minutes) and long-term (15, 30, 45, and 60 minutes) events. Given that C80 procedures have an average duration of 38 minutes and AL21 procedures average 66 minutes, extending phase predictions up to 60 minutes captures most of the workflow. This range enables us to simultaneously predict immediate transitions and estimate the remaining surgery duration.

Classification Task. Since long-term future phase classification has not been studied in previous work, direct comparisons to other surgical workflow anticipation methods are not possible. Therefore, we assess our generative approaches against two baseline methods: a simple continuation model (Naive1) and a probabilistic prediction model (Naive2). **Naive1** baseline extends the current recognised class over the future predicted horizon for H minutes. While effective for short-term predictions, its performance naturally degrades over time with new class transitions. **Naive2** baseline predicts future phases by sampling from the probability distribution P_{i,j,n_i-60} , conditioned on the predicted current class i and the anticipated future index n_i . This baseline is effective due to the strong priors inherent in structured workflows, leveraging high recognition accuracy and precisely defined anticipation times.

Regression Task. We include a secondary evaluation to compare our method to previous works. Specifically, we benchmark against Bayesian [12] and IIA-Net [13], both predicting the remaining time until the next phase occurrence. IIA-Net relies on instrument presence and phase labels for supervision, while we solely use the latter. We did not include results from the Trans-SVNet [34] method as their evaluation was limited to a single horizon (5 minutes) and did not report the weighted MAE score (see Sec. 3.4). We extend the phase anticipation regression task to long horizons to include the remaining surgery duration (RSD) evaluation following previous works [7, 9, 10].

3.4 Evaluation Metrics

We use a combination of classification and regression metrics to evaluate our methodology. These metrics are calculated for each anticipation time, allowing us to analyse the model’s performance through time. We use frame-based accuracy to measure the proportion of correctly classified frames among all predictions. Although the videos are untrimmed with preserved class distribution from full surgeries, we still provide class-based metrics (F1-score, Precision, and Recall) over extended time horizons in the supplementary materials to assess performance on less frequent phases. Finally, we use the Mean Absolute Error (MAE) to evaluate the model’s performance on the regression task, specifically for predicting the remaining time until the next phase occurrence. This metric quantifies the average absolute prediction errors in minutes. We use the *wMAE*, *inMAE*, and *outMAE* for *weighting* samples *outside* and *inside* the temporal horizon as proposed in [12, 13], respectively. We select the best model based on the mean accuracy and wMAE over each task’s time intervals.

4 Results

4.1 Surgical Phase Anticipation

Table 1 summarises the classification results for phase recognition at and anticipation at specific future time points τ_5 and τ_{15} , where $\tau_i = t + n_i \cdot 60$ (in minutes). Results are reported for both Cholec80 and AutoLaparo21 datasets.

Table 1: Surgical Phase Anticipation. Acc_{τ_t} : phase anticipation at time t (in minutes). Acc_{τ_v} : mean accuracy for all anticipation time steps.

Methods	Cholec80 (40/40)				AutoLaparo21 (14/7)			
	Acc_{τ_0}	Acc_{τ_5}	$Acc_{\tau_{15}}$	Acc_{τ_v}	Acc_{τ_0}	Acc_{τ_5}	$Acc_{\tau_{15}}$	Acc_{τ_v}
Naive1 †	<u>90.9</u>	47.5	12.0	32.2	<u>78.0</u>	<u>52.0</u>	15.2	35.5
Naive2 †	<u>90.9</u>	49.0	44.1	47.8	<u>78.0</u>	45.2	35.6	41.9
SWAG-AR	90.4	<u>56.4</u>	29.4	44.7	75.5	51.0	21.5	38.1
SWAG-SP	89.0	43.7	46.4	45.8	75.7	51.1	44.8	48.1
SWAG-SP*	89.8	51.5	<u>47.0</u>	<u>49.5</u>	74.4	51.4	<u>45.3</u>	49.8
SWAG-SP-R2C	90.9	59.6	54.5	56.6	78.0	52.1	46.0	<u>47.5</u>

Note: The light blue cells in bold and underlined values are the best and second-best results, respectively. * indicates the presence of our prior knowledge token embedding initialization method. † indicates models that were only supervised on the recognition task (Acc_{τ_0}).

On average over *all* horizons Acc_{τ_V} , SWAG-SP-R2C achieves superior performance on Cholec80 and ranks second on AutoLaparo21. Figure 3 shows that SWAG-SP-R2C and SWAG-SP* outperform other methods and baselines on both datasets over an 18-minute horizon. SWAG-SP* shows a marked improvement in accuracy, highlighting the value of our prior knowledge embedding strategy, especially on Cholec80. The relatively strong performance of Naive2 and SWAG-SP* on Cholec80 compared to AutoLaparo21 likely reflects a more uniform probability distribution of possible future phases in the AutoLaparo21 dataset.

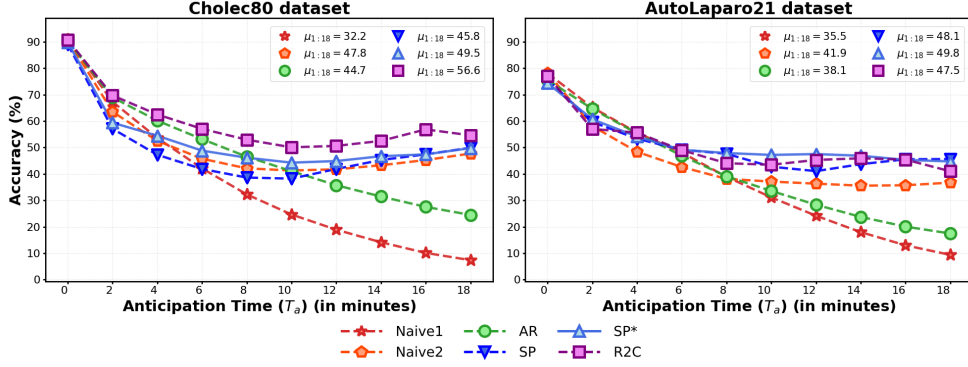


Fig. 3: Model performance (accuracy) of surgical phase recognition and anticipation on Cholec80 and AutoLaparo21 up to 18 minutes, with mean values over 18 minutes.

4.2 Surgical Phase Anticipation with Remaining Time

Based on the stronger classification results from the single-pass approaches i.e. SWAG-SP* and SWAG-SP-R2C, we select the single-pass (SWAG-SP) decoder for comparison on state-of-the-art methods on the remaining time until the next phase occurrence regression task (see Table 2).

Table 2: Remaining time to next phase occurrence at 2, 3, and 5 minutes horizons. MAEs (in minutes) for *inside* and *outside* the anticipation window, and *weighted* mean. The results from previous methods are reported in IIA-Net [13].

Methods	Cholec80 (60-20)								
	$wMAE[\downarrow]$			$inMAE[\downarrow]$			$outMAE[\downarrow]$		
	2 min	3 min	5 min	2 min	3 min	5 min	2 min	3 min	5 min
Bayesian[12]	0.39	0.59	0.85	0.63	0.86	<u>1.17</u>	0.15	0.32	0.52
IIA-Net [13] †	<u>0.36</u>	0.49	0.68	<u>0.62</u>	<u>0.81</u>	1.08	0.10	0.18	0.28
SWAG-SP	0.32	0.48	<u>0.80</u>	0.54	0.77	1.26	0.09	0.17	<u>0.34</u>

Note: The light blue cells in bold and underlined values are the best and second-best results, respectively. † indicates methods using more data annotations for supervision i.e. bounding boxes and segmentation masks.

For 2-minute and 3-minute horizons, SWAG-SP achieves the best inMAE scores (0.54 and 0.77 minutes for 2 and 3 minutes), outperforming Bayesian [12] and IIA-Net [13]. At the 5-minute horizon, SWAG-SP ranks second with its wMAE score, showing strong adaptability for mid-range anticipations. IIA-Net [13] uses additional manual annotations like instrument bounding boxes and segmentation maps for supervision, while our approach relies solely on phase labels.

In Table 3, we compare our SWAG-SP method with previous approaches on the Remaining Surgery Duration (RSD) task. Using 4-fold cross-validation, our model ranks second on MAE-5 and MAE-ALL, outperforming previous methods, except BD-Net, all methods exclusively designed for this task. These results underscore our model’s versatility across several benchmarks.

Table 3: Remaining Surgery Duration (RSD) estimation on Cholec80. Those results were reported in BD-Net.

Methods	MAE-5 (min)	MAE-30 (min)	MAE-ALL (min)
TimeLSTM [6]	3.00 ± 1.87	5.30 ± 1.86	8.27 ± 6.25
RSDNet [7]	8.36 ± 3.71	6.83 ± 2.57	10.01 ± 6.54
CataNet [9]	2.47 ± 2.62	5.53 ± 2.75	8.27 ± 6.81
BD-Net [10]*	1.97 ± 1.54	4.84 ± 2.31	7.75 ± 6.43
SWAG-SP (ours)	2.24 ± 2.32	6.48 ± 3.85	8.18 ± 5.33

Note: * This method randomly created 4-splits for validation, whereas we used consecutive 60/20 splits for training and testing, respectively.

Fig. 4 illustrate a more practical representation of our approach, seamlessly extending the well-established phase recognition task with our generative-based anticipation framework. We show how the remaining time predictions per class (last eight rectangles) can be stacked into a 1-dimensional future segment (transparent) after the recognised surgical phases in an online manner (red dashed vertical line).

We show additional qualitative results and extended ablations in the supplementary materials (Sec. 1 in SM).

5 Discussion

Our study evaluates methods for anticipating future surgical phases using transformer-based generative approaches. We investigate two decoding approaches: single-pass (SWAG-SP) and auto-regressive (SWAG-AR). We then demonstrate how prior knowledge can be used to initialise future tokens in single-pass decoding (SWAG-SP*), resulting in improved performance. Additionally, we show how the remaining time prediction task with the single-pass model (SWAG-SP) can be extended to a classification task (SWAG-SP-R2C).

While the auto-regressive (SWAG-AR) model works well for short-term phase anticipation, its performance declines over longer horizons, accumulating errors over time. Our results show that SWAG-SP achieves the lowest wMAE and inMAE for up to 5-minute horizons, outperforming both the Bayesian model [12] and IIA-Net [13]. While the Bayesian model provides uncertainty estimation, it lacks short-term precision, and IIA-Net’s reliance on bounding boxes and segmentation masks may limit

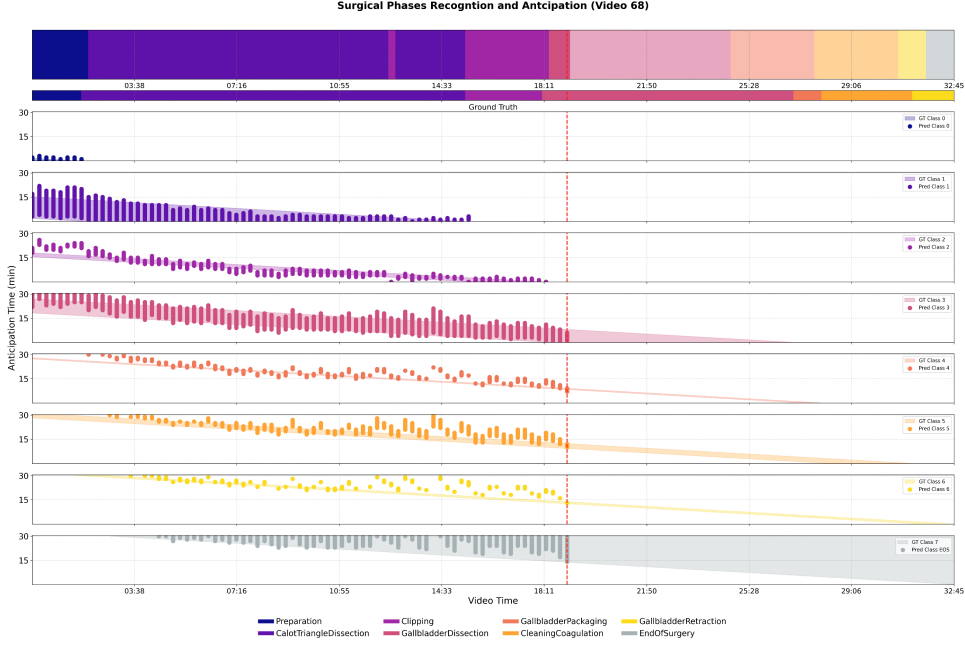


Fig. 4: Surgical phase recognition and anticipation within a 30-minute horizon (y-axis) for Cholec80’s video 68, with the current elapsed time (x-axis) indicated by the red dashed vertical line. The thin, second row shows the ground truth phase segments, while the top rectangle displays the classified frames into phases; note that the more transparent colours to the right of the dashed line indicate the generated future phases at 60-second intervals. Each per-class regressed vertical segment is mapped onto a 1D timeline for both past and future. The last eight rectangles illustrate the regression-to-classification predictions per class.

its scaling feasibility. We then extend the anticipation horizon beyond the previous 5-minute horizon to 15, 30, 45, and 60 minutes, bridging into the remaining surgery duration (RSD) prediction task, ranking second, while not making specific changes to the model.

Although our experiments indicate that using single-pass decoding with remaining time regression supervision achieves comparable quantitative performance to class-based generative approaches (SWAG-AR and SWAG-SP*), sequence generation offers the advantage of predicting repeated class occurrences within a single horizon, enabling the generation of fine-grained action sequences in a procedure. While the ability to predict multiple class occurrences within a sequence enhances model flexibility, it also increases the risk of misclassification on workflows with many class types and transitions. Cholecystectomies in Cholec80 follow a more standardised protocol with stronger phase ordering and fewer class repetitions [32], making transitions more predictable. In contrast, AutoLaparo21 exhibits greater variability in phase ordering and

repetition [33]. While both datasets contain the same number of phase classes, these structural differences likely impact anticipation performance.

Real-time phase anticipation can alleviate the cognitive load on surgical teams and support intraoperative decision-making by offering foresight into upcoming phases over whole surgeries. This predictive support could improve team coordination, reduce surgery times, and enhance patient safety. Nevertheless, for wide clinical acceptance, future approaches must incorporate robust uncertainty estimation, as exemplified by the Bayesian perspective [12].

However, precise intraoperative workflow timing prediction faces intrinsic challenges due to anatomical differences, surgeon skill, patient-specific factors, and real-time changes. Surgery is not entirely deterministic, with multiple possible paths leading to optimal outcomes, making accurate long-term prediction especially challenging for generative models, especially with few training samples. We therefore distinguish two perspectives: (1) anticipating a surgeon’s future surgical workflow intraoperatively, which is highly variable over long horizons, offers limited accuracy even for high-level events like surgical phases, when trained on small datasets, as demonstrated by our results ($\simeq 50\%$), and (2) generating plausible future workflows derived from annotated surgical videos. Even if surgery is infinitely complex to predict in a time-sensitive manner, our SWAG approach could provide valuable guidance in structured scenarios. Moving forward, we believe that future methods should adopt a more open-ended, generative perspective, accommodating multiple plausible surgical workflow trajectories that can all provide optimal outcomes for the patient rather than assuming a single valid path.

6 Conclusion

In this work, we introduced SWAG, a novel model unifying surgical phase recognition and long-term generative-based anticipation within a single encoder-decoder framework enhanced by successfully embedding prior knowledge in future-generated tokens. Evaluations on the Cholec80 and AutoLaparo21 datasets demonstrate that SWAG outperforms naive baselines in classification and achieves competitive results in regression tasks, specifically for remaining surgery duration predictions. To support its clinical integration, we have demonstrated SWAG’s utility within a software application¹. This work establishes SWAG as a novel framework in surgical workflow anticipation to support intraoperative guidance.

Declarations

The authors declare no conflict of interest. This article does not contain any studies with human participants or animals performed by any of the authors. This manuscript does not contain any patient data.

¹<https://maxboels.github.io/swag>

References

- [1] Sexton, K., Johnson, A., Gotsch, A., Hussein, A.A., Cavuoto, L., Guru, K.A.: Anticipation, teamwork and cognitive load: chasing efficiency during robot-assisted surgery. *BMJ Quality & Safety* (2018)
- [2] Yurko, Y.Y., Scerbo, M.W., Prabhu, A.S., Acker, C.E., Stefanidis, D.: Higher mental workload is associated with poorer laparoscopic performance as measured by the nasa-tlx tool. *Simulation in Healthcare* (2010)
- [3] Czempiel, T., Paschali, M., Keicher, M., Simson, W., Feußner, H., Kim, S.T., Navab, N.: Tecno: Surgical phase recognition with multi-stage temporal convolutional networks. *International Conference on Medical Image Computing and Computer-Assisted Intervention* (2020)
- [4] Liu, Y., Boels, M., García-Peraza-Herrera, L.C., Vercauteren, T.K.M., Dasgupta, P., Granados, A., Ourselin, S.: Lovit: Long video transformer for surgical phase recognition. *Medical Image Analysis* (2023)
- [5] Liu, Y., Huo, J., Peng, J., Sparks, R., Dasgupta, P., Granados, A., Ourselin, S.: Skit: a fast key information video transformer for online surgical phase recognition. In: *Proceedings of the IEEE/CVF International Conference on Computer Vision* (2023)
- [6] Aksamentov, I., Twinanda, A.P., Mutter, D., Marescaux, J., Padoy, N.: Deep neural networks predict remaining surgery duration from cholecystectomy videos. In: *Medical Image Computing and Computer-Assisted Intervention - MICCAI 2017*, pp. 586–593. Springer, Cham (2017)
- [7] Twinanda, A.P., Yengera, G., Mutter, D., Marescaux, J., Padoy, N.: Rsdnet: Learning to predict remaining surgery duration from laparoscopic videos without manual annotations. *IEEE transactions on medical imaging* (2018)
- [8] Rivoir, D., Bodenstedt, S., Bechtolsheim, F., Distler, M., Weitz, J., Speidel, S.: Unsupervised temporal video segmentation as an auxiliary task for predicting the remaining surgery duration. In: *OR 2.0 Context-Aware Operating Theaters and Machine Learning in Clinical Neuroimaging*, pp. 29–37. Springer, Cham (2019)
- [9] Marafioti, A., Hayoz, M., Gallardo, M., Márquez Neila, P., Wolf, S., Zinkernagel, M., Sznitman, R.: Catanet: Predicting remaining cataract surgery duration. In: *Medical Image Computing and Computer Assisted Intervention – MICCAI 2021*, pp. 426–435. Springer, Cham (2021)
- [10] Wu, J., Zou, X., Tao, R., Zheng, G.: Nonlinear regression of remaining surgery duration from videos via bayesian lstm-based deep negative correlation learning. *Computerized Medical Imaging and Graphics* (2023)

- [11] Wijekoon, A., Das, A., Herrera, R.R., Khan, D.Z., Hanrahan, J., Carter, E., Luoma, V., Stoyanov, D., Marcus, H.J., Bano, S.: Pitrsdnet: Predicting intra-operative remaining surgery duration in endoscopic pituitary surgery. arXiv preprint arXiv: 2409.16998 (2024)
- [12] Rivoir, D., Bodenstedt, S., Funke, I., Bechtolsheim, F., Distler, M., Weitz, J., Speidel, S.: Rethinking anticipation tasks: Uncertainty-aware anticipation of sparse surgical instrument usage for context-aware assistance. *International Conference on Medical Image Computing and Computer-Assisted Intervention* (2020)
- [13] Yuan, K., Holden, M., Gao, S., Lee, W.: Anticipation for surgical workflow through instrument interaction and recognized signals. *Medical Image Analysis* (2022)
- [14] Radford, A., Wu, J., Child, R., Luan, D., Amodei, D., Sutskever, I.: Language models are unsupervised multitask learners. *OpenAI blog* (2019)
- [15] Wang, J., Chen, G., Huang, Y., Wang, L., Lu, T.: Memory-and-anticipation transformer for online action understanding. *IEEE International Conference on Computer Vision* (2023) <https://doi.org/10.1109/ICCV51070.2023.01271>
- [16] Blum, T., Feußner, H., Navab, N.: Modeling and segmentation of surgical workflow from laparoscopic video. In: *Medical Image Computing and Computer-Assisted Intervention – MICCAI 2010*, pp. 400–407. Springer, Berlin, Heidelberg (2010)
- [17] Twinanda, A.P.: Vision-based approaches for surgical activity recognition using laparoscopic and RGBD videos. PhD thesis, University of Strasbourg (2017)
- [18] Vaswani, A., Shazeer, N.M., Parmar, N., Uszkoreit, J., Jones, L., Gomez, A.N., Kaiser, L., Polosukhin, I.: Attention is all you need. *Neural Information Processing Systems* (2017)
- [19] Dosovitskiy, A., Beyer, L., Kolesnikov, A., Weissenborn, D., Zhai, X., Unterthiner, T., Dehghani, M., Minderer, M., Heigold, G., Gelly, S., Uszkoreit, J., Houlsby, N.: An image is worth 16x16 words: Transformers for image recognition at scale. *International Conference on Learning Representations* (2020)
- [20] Gao, X., Jin, Y., Long, Y., Dou, Q., Heng, P.: Trans-svnet: Accurate phase recognition from surgical videos via hybrid embedding aggregation transformer. In: Bruijne, M., Cattin, P.C., Cotin, S., Padoy, N., Speidel, S., Zheng, Y., Essert, C. (eds.) *Medical Image Computing and Computer Assisted Intervention - MICCAI 2021*. Springer, ??? (2021)
- [21] Ding, X., Li, X.: Exploring segment-level semantics for online phase recognition from surgical videos. *IEEE Trans. Medical Imaging* **41**(11), 3309–3319 (2022)

- [22] Rivoir, D., Funke, I., Speidel, S.: On the pitfalls of batch normalization for end-to-end video learning: A study on surgical workflow analysis. *Medical Image Analysis* **94**, 103126 (2024) <https://doi.org/10.1016/j.media.2024.103126>
- [23] Yang, S., Luo, L., Wang, Q., Chen, H.: Surgformer: Surgical transformer with hierarchical temporal attention for surgical phase recognition. *International Conference on Medical Image Computing and Computer-Assisted Intervention* (2024) <https://doi.org/10.48550/arXiv.2408.03867>
- [24] Ban, Y., Rosman, G., Eckhoff, J., Ward, T.M., Hashimoto, D., Kondo, T., Iwaki, H., Meireles, O., Rus, D.: Supr-gan: Surgical prediction gan for event anticipation in laparoscopic and robotic surgery. *IEEE Robotics and Automation Letters* (2021) <https://doi.org/10.1109/lra.2022.3156856>
- [25] Boels, M., Liu, Y., Dasgupta, P., Granados, A., Ourselin, S.: Supra: Surgical phase recognition and anticipation for intra-operative planning. *arXiv preprint arXiv: 2403.06200* (2024)
- [26] Zhang, X., Moubayed, N.A., Shum, H.P.H.: Towards graph representation learning based surgical workflow anticipation. *IEEE-EMBS International Conference on Biomedical and Health Informatics (BHI)* (2022) <https://doi.org/10.1109/BHI56158.2022.9926801>
- [27] Yin, L., Ban, Y., Eckhoff, J., Meireles, O., Rus, D., Rosman, G.: Hypergraph-transformer (hgt) for interactive event prediction in laparoscopic and robotic surgery. *arXiv preprint arXiv: 2402.01974* (2024)
- [28] Ginesi, M., Meli, D., Roberti, A., Sansonetto, N., Fiorini, P.: Autonomous task planning and situation awareness in robotic surgery. *IEEE/RJS International Conference on Intelligent RObots and Systems* (2020)
- [29] Qin, Y., Feyzabadi, S., Allan, M., Burdick, J., Azizian, M.: davincinet: Joint prediction of motion and surgical state in robot-assisted surgery. *IEEE/RJS International Conference on Intelligent RObots and Systems* (2020)
- [30] Zhang, J., Zhou, S., Wang, Y., Shi, S., Wan, C., Zhao, H., Cai, X., Ding, H.: Laparoscopic image-based critical action recognition and anticipation with explainable features. *IEEE Journal of Biomedical and Health Informatics* (2023)
- [31] Girdhar, R., Grauman, K.: Anticipative video transformer. *IEEE International Conference on Computer Vision* (2021) <https://doi.org/10.1109/ICCV48922.2021.01325>
- [32] Twinanda, A.P., Shehata, S., Mutter, D., Marescaux, J., Mathelin, M., Padoy, N.: Endonet: A deep architecture for recognition tasks on laparoscopic videos. *IEEE Trans. Medical Imaging* **36**(1), 86–97 (2017)

- [33] Wang, Z., Lu, B., Long, Y., Zhong, F., Cheung, T.-H., Dou, Q., Liu, Y.: Autolaparo: A new dataset of integrated multi-tasks for image-guided surgical automation in laparoscopic hysterectomy. In: International Conference on Medical Image Computing and Computer-Assisted Intervention, pp. 486–496 (2022). Springer
- [34] Jin, Y., Long, Y., Gao, X., Stoyanov, D., Dou, Q., Heng, P.-A.: Trans-svnet: hybrid embedding aggregation transformer for surgical workflow analysis. International Journal of Computer Assisted Radiology and Surgery (2022)
- [35] Chen, Z., Luo, X., Wu, J., Chan, D., Lei, Z., Wang, J., Ourselin, S., Liu, H.: Vs-assistant: Versatile surgery assistant on the demand of surgeons (2024)

7 Supplementary Material

7.1 Implementation Details

Our experiments were conducted on a single NVIDIA Tesla V100 GPU. We used a 12-head, 12-layer Transformer encoder as our spatial feature extractor, based on the ViT-B/16 architecture following LoViT [4]. This model was pre-trained on ImageNet 1K (IN1k) and produced 768-d representations, with an input image size of 248×248 pixels. For training the spatial feature extractor, we used stochastic gradient descent with momentum for 35 epochs, with a 5-epoch warm-up period and a 30-epoch cosine annealed decay. We used a batch size of 16 and a learning rate of 0.1, which was multiplied by 0.1 at the 20th and 30th epochs. We set the weight decay to $1e-4$ and the momentum to 0.9. For the Temporal Self-Attention, we used an input clip length l of 1440 frames or 24 minutes at 1fps with a sliding context length window w of 20 frames, generating 512-d feature vectors. Key-pooled feature dimensions d are 64-d and 32-d on Cholec80 and AutoLaparo21, respectively. The temporal modules underwent training for 40 epochs using SGD and momentum with a learning rate of $3e-4$, weight decay of $1e-5$, a 5 epoch warm-up period, and a 35 epoch cosine annealed decay, with a batch size of 8.

7.2 Future Tokens Embedding Initialization

This process involves generating a final input embedding \mathbf{x}_τ for each future token τ by combining the initial embedding \mathbf{e}_τ , the probability vector \mathbf{p}_τ projected into a higher-dimensional space, and a sinusoidal positional encoding, ultimately forming the input for the transformer decoder.

$$\mathbf{p}_\tau = \mathbf{P}_{i,:,\tau} \quad \text{for } \tau = 1, 2, \dots, 15 \quad (2)$$

$$\mathbf{h}_\tau = W_p \mathbf{p}_\tau + \mathbf{b}_p \quad (3)$$

$$\mathbf{x}_\tau = \text{LayerNorm}(\mathbf{e}_\tau + \alpha \mathbf{h}_\tau + \text{PositionalEncoding}(\tau)) \quad (4)$$

7.3 Ablation Studies

We conducted ablation experiments to study the impact of various factors on model performance, including context length, anticipation interval, number of context tokens, temporal pooling methods, and model size.

Context Length. Figure 5 shows that a context length of 24 minutes yields the highest mean cumulative accuracy on both datasets.

Compression and Anticipation Time. Figure 6 indicates that a 1-minute interval between input samples produces the highest accuracies on both datasets.

Temporal Pooling Methods. Figure 7 compares global and interval pooling methods. Single-pass decoding with global context tokens consistently outperforms auto-regressive decoding with either temporal pooling methods for all numbers of context tokens and on both datasets.

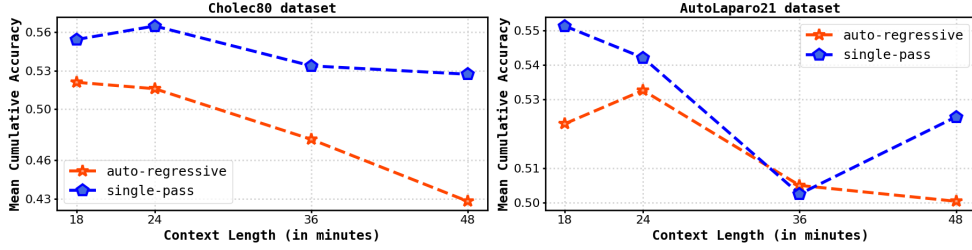


Fig. 5: Context Length (in minutes) of the input sequence.

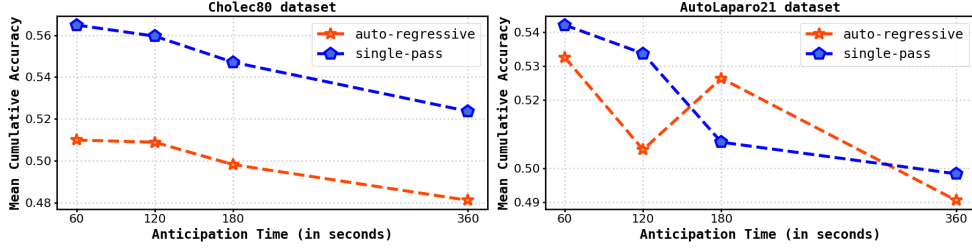


Fig. 6: Effect of the anticipation time between frames during training (in seconds) on the test accuracy.

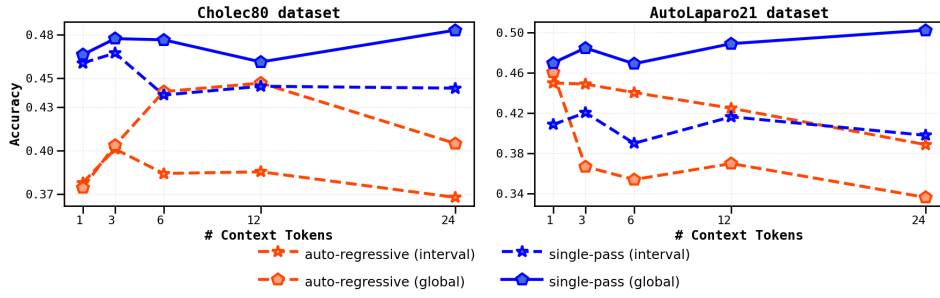


Fig. 7: Number of context tokens with a fixed context length of 24 minutes i.e. compression of input sequence with global and interval temporal pooling methods.

Model Size. Figure 8 demonstrates that medium-sized models achieve the best overall accuracies, with the optimal model size varying slightly between datasets. These ablations indicate that careful tuning of these parameters can significantly impact long-term surgical phase anticipation performance.

Inside horizon MAE per class. On the Cholec80 dataset, we observe an increasing error from approximately 2 to 8 minutes for mid- to late-stage surgical phases, specifically classes 4, 5, 6, and EOS. In contrast, anticipation errors for phases 2 and

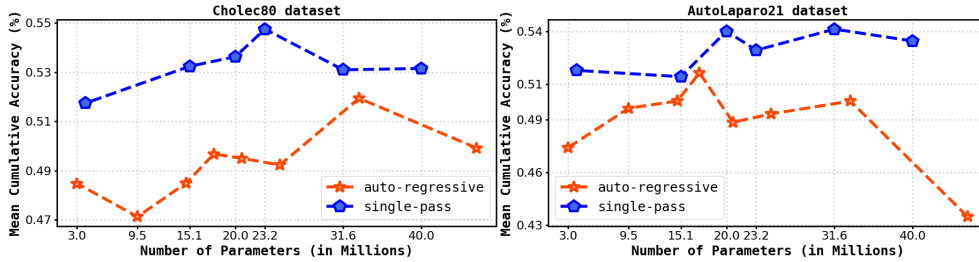


Fig. 8: Model size (million parameters) over accuracy.

3 remain stable over time, averaging around 5.5 minutes. The model exhibits an error below 1 minute for phase 1, likely because phase 1 occurs at the very beginning of the surgery, leading the model to predict low values that are often accurate.

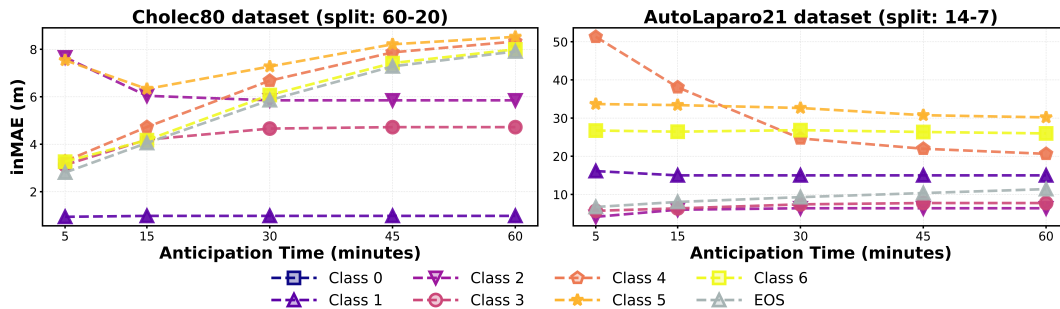


Fig. 9: MAEs inside the anticipation horizons per-class on Cholec80 and AutoLaparo21.

For the AutoLaparo21 dataset, the task is more challenging, especially for mid- to late-phase stages, though the EOS class is less impacted. Errors are less correlated with time, reflecting the intrinsic uncertainty of phase variability. Classes 4, 5, and 6, in particular, are inconsistently present and often exhibit abrupt transitions, making prediction difficult. Over long horizons, the model takes a conservative approach by predicting mid-range values. However, as it nears the 5-minute horizon, it attempts to predict lower, more specific values, which can lead to substantial errors if the phase is absent or has sudden transitions.

Standard Deviation. To assess the stability and robustness of the models, we depict the standard deviation of the anticipation accuracies across different videos. As shown in Fig. 10, the single-pass method has a lower variance on Cholec80 and, conversely, a higher variance on AutoLaparo21.

Class-based Metrics. We show the F1, Precision, and Recall evaluation metrics in Fig. 11, although we argue that the class distribution is well-balanced as our testing videos correspond to real surgeries.

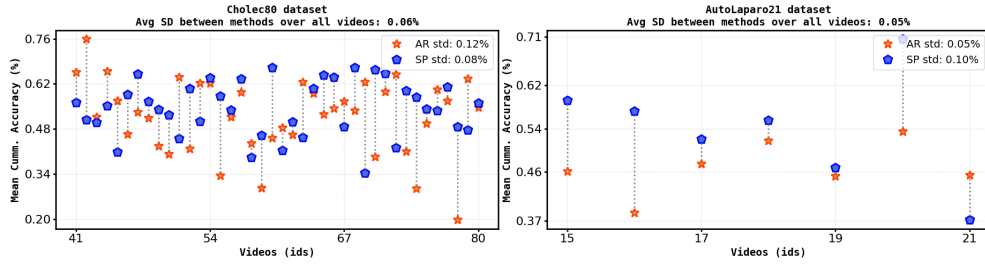


Fig. 10: Standard Deviation between videos accuracy.

7.4 Additional Quantitative Results

The SP* and R2C models remain the top two performing methods across all anticipation time steps.

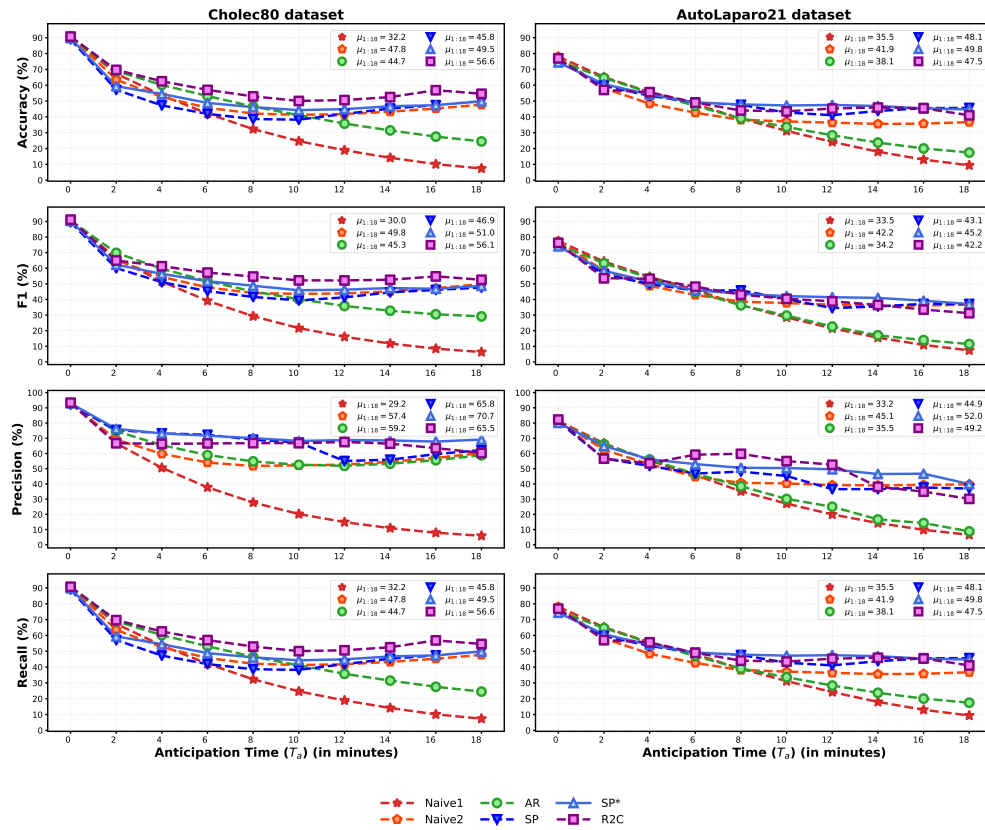


Fig. 11: Evaluation metrics for each method on both datasets: Accuracy, F1, Precision, and Recall.

7.5 Additional Qualitative Results

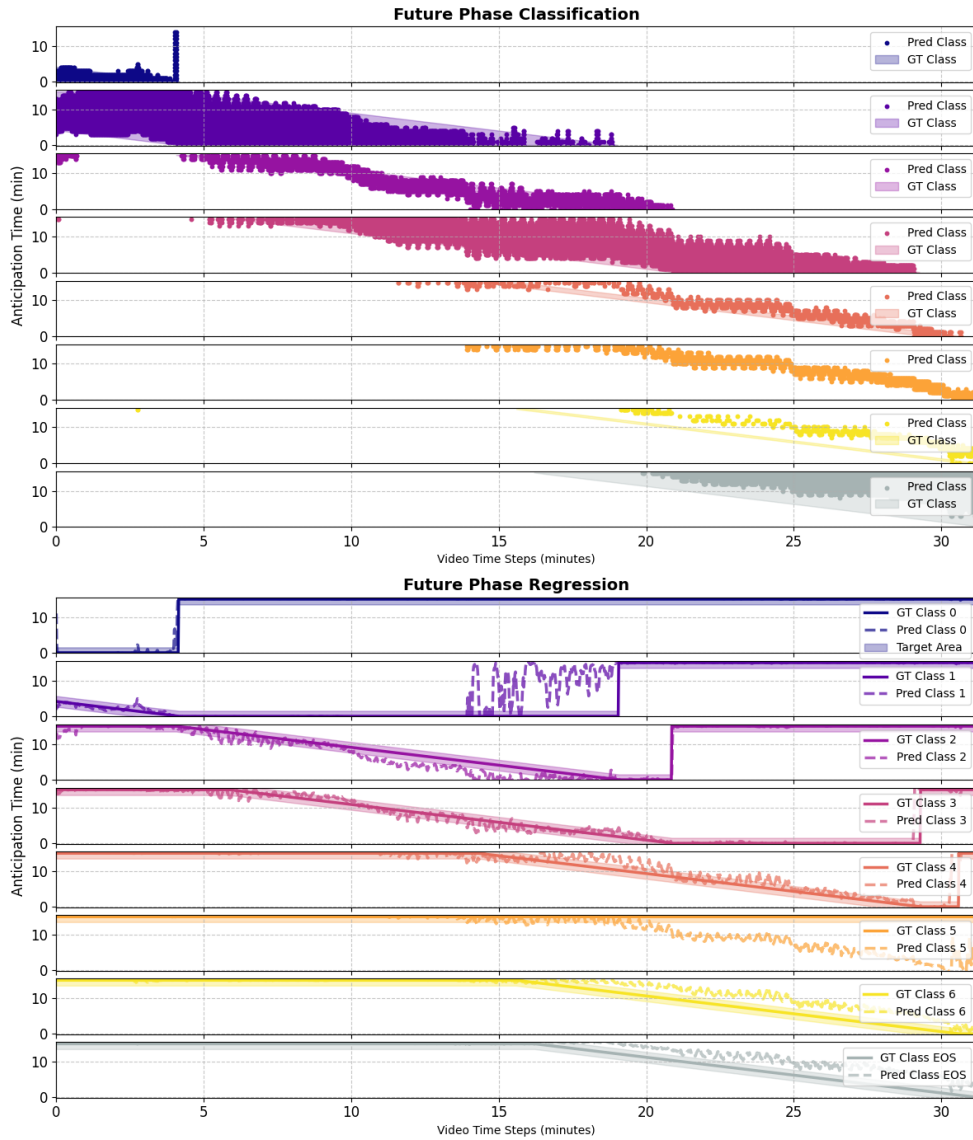


Fig. 12: Comparison of future phases classification (top) and regression (bottom) task on video 65 from the cholec80 dataset.

Figure 13 presents a comparative visualization of the regression and classification tasks applied to surgical phase anticipation. In the regression task, the model estimates the remaining time until the next occurrence of each phase, while the classification

task predicts classes at future discretized time points. We illustrate the performance of SP* in comparison with the ground truth in Fig. 13.

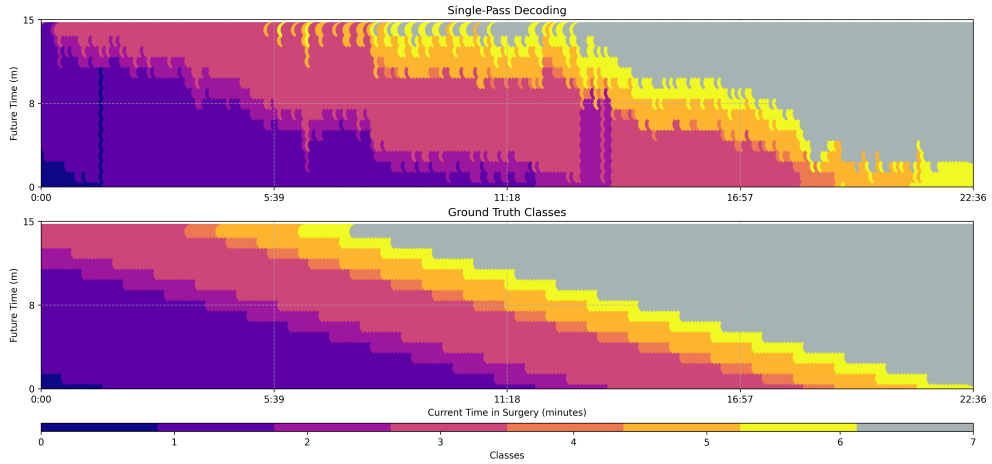


Fig. 13: SWAG-SP* predictions (top) versus ground truth (bottom) surgical phase recognition and anticipation of up to 15 minutes (y-axis) of a Cholec80’s video 73 current elapsed time (x-axis). Each colour represents a distinct phase class.

7.6 Our SWAG Application

We show how a pre-trained language model can translate the predictions into language. Previous works use a similar approach but for the recognition task [35]. Available on our project homepage: <https://maxboels.github.io/swag>

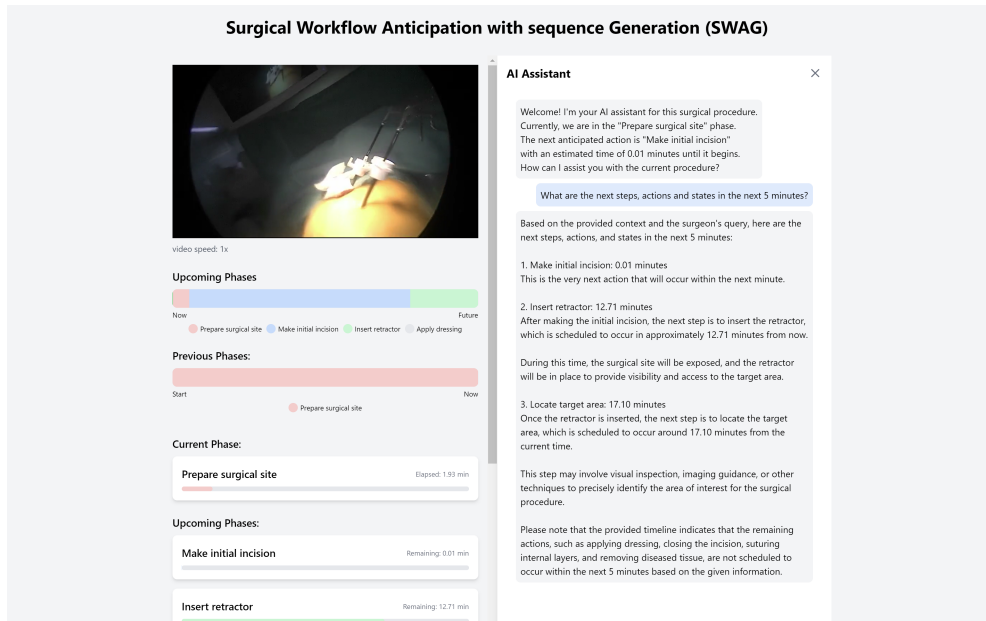


Fig. 14: SWAG + LLM application.